# Diffusion and Crystallization of Dichloromethane within the Pores of Amorphous Solid Water

Radha Gobinda Bhuin, Rabin Rajan J. Methikkalam, Soumabha Bag, and Thalappil Pradeep*

DST Unit of Nanoscience and Thematic Unit of Excellence, Department of Chemistry, Indian Institute of Technology Madras, Chennai 600 036, India

S *Supporting Information*

ABSTRACT: Dichloromethane (CH_2Cl_2) thin films deposited on Ru(0001) at low temperatures ($\sim$80 K or lower) undergo a phase transition at $\sim$95 K, manifested by the splitting of its wagging mode at 1265 cm^{-1}, due to factor group splitting. This splitting occurs at relatively higher temperatures ($\sim$100 K) when amorphous solid water (ASW) is deposited over it, with a significant reduction in intensity of the high-wavenumber component (of the split peaks). Control experiments showed that the intensity of the higher wavenumber peak is dependent on the thickness of the water overlayer. It is proposed that diffusion of CH_2Cl_2 into ASW occurs and it crystallizes within the pores of ASW, which increases the transition temperature. However, the dimensions of the CH_2Cl_2 crystallites get smaller with increasing thickness of ASW with concomitant change in the intensity of the factor group split peak. Control experiments support this suggestion. We propose that the peak intensities can be correlated with the porosity of the ice film. Diffusion of CH_2Cl_2 has been supported by low-energy Cs$^+$ scattering and temperature-programmed desorption spectroscopies.
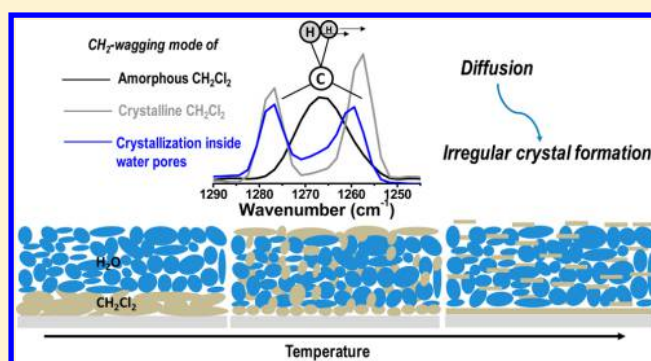
INTRODUCTION

Molecules deposited at low temperatures on cold surfaces are generally amorphous in nature with randomly oriented structure. The amorphous form of the molecules may undergo a structural change upon annealing to higher temperature to form their most stable crystalline structures. Study of such phase transitions of molecular solids is a salient area of research due to their importance in phenomena ranging from environmental to biological and interstellar science. Different phases of molecular solids provide unique physical and chemical environment. This is a vast area of research, and phase transition of different molecules has been investigated in great detail.[1−4] Techniques used for this study are mostly spectroscopic and scattering methods, namely, X-ray diffraction,[5] low-energy electron diffraction (LEED),[6] electron diffraction,[7] transmission electron microscopy (TEM),[8] low-energy ion collisions,[9,10,11] and most commonly by infrared (IR) spectroscopy.[1,3,4] The last one in this list has been utilized to study phase transitions in water-ice,[1,3] methanol-ice,[2] and many other molecular solids.[4,12−14] Although dichloromethane is one of the most frequently used organic solvents in the laboratory, the phase transition of this molecule is not well-understood. In 1970, the crystal structure of dichloromethane has been predicted from an IR spectroscopic study.[15] However, to best of our knowledge, there is no report on the phase transition of this molecule and also no report has been found on the IR spectrum of amorphous dichloromethane. Study of

this molecule is also important in the context of stratospheric chemistry. Chloromethanes present in this environment interact with water-ice particles, eventually causing the depletion of the ozone layer. Water-ice surface plays a catalytic role in this process.[16] Several theoretical and experimental studies have also been performed on halomethane/water-ice system.[17−20]

From a fundamental point of view, water-ice is a model system for molecular solids to study elementary processes. Water-ice can exist in many different structural forms, depending on its formation. Mainly two different forms of water-ice (crystalline and amorphous) can be generated in vacuum on a cold surface at different temperatures by vapor deposition. In the universe the amorphous form of water-ice, known as amorphous solid water (ASW), is dominant.

ASW is highly porous in nature. Porosity of water-ice governs elementary processes like diffusion,[21,22] adsorption of gaseous species,[17,21,22] rapid desorption of trapped gases (termed as molecular volcano),[18] phase transition,[23] tunneling reactions,[21] etc. Various factors such as local temperature,[7] incident molecular flux,[3] incident angle,[24−26] and kinetic energy[27] affect the porosity of water-ice. Thus, a number of studies have been carried out to probe porous ASW. Temperature-programmed

desorption (TPD) experiments have been used extensively in these cases.[28−30] Diffusion and adsorption of molecules through the pores of ASW have also been investigated to a large extent by TPD. Limited reports exist where spectroscopic methods, such as IR spectroscopy, have been utilized to understand the diffusion of molecules through water-ice.[25,31,32] Moreover, there are no reports on the spectroscopic properties of the diffused molecules. It is fundamentally important to study diffusion and interactions of molecules with ASW, which determine the composition and outgassing kinetics of the extraterrestrial ices.[2]

In this present study, we report two important investigations. First, we investigate the phase transition of pure dichloromethane in ultrahigh vacuum (UHV) and, second, the fate of crystallization of this molecule in the presence of ASW. Surface-sensitive reflection absorption infrared (RAIR) spectroscopy was used to understand the phase transition of pure dichloromethane. It was also observed that, in the presence of ASW, the molecules diffused through the pores of ASW and crystallize inside the pores to form irregular crystallites. The phenomenon is further supported by TPD and extremely surface-sensitive Cs$^+$ scattering experiments.

■ EXPERIMENTAL SECTION

All the experiments were carried out using a custom-built instrument. A detailed description of the instrument is given elsewhere.[33] Briefly, the instrument consists of three UHV chambers (fully made of nonmagnetic stainless steel) composed of an ionization chamber (IC), an octupole chamber, and a scattering chamber; the sample manipulator with closed cycle He cryostat is mounted on the latter. Each vacuum chamber is differentially pumped by a turbomolecular pump (TMP). A diaphragm pump backs the ionization chamber TMP, and the octupole and scattering chamber TMPs are pumped by a TMP, again backed by a diaphragm pump. The base pressure of the instrument in the scattering chamber is 8×10^{-10} mbar. A Bayard−Alpert-type (B−A) gauge is employed to measure the pressure reading in each chamber. The vacuum components and gauges are procured from Pfeiffer Vacuum GmbH. Mass spectrometer components were from Extrel CMS. The instrument is capable of performing mass-selected low-energy (1−100 eV) ion scattering, low-energy (2−1000 eV) alkali ion scattering, RAIRS, and TPD spectroscopy. A unique aspect of this instrument is ultralow-energy (in the range of 1 eV) ion scattering, although such experiments were not used for the present work. RAIRS was employed to understand diffusion and crystallization of dichloromethane within ASW pores. In the scattering chamber of our instrument, thin films of molecular solids were grown layer by layer on a polished Ru(0001) single crystal. The single (Ru) crystal is in turn mounted on a copper holder that is connected to a closed cycle He cryostat (from ColdEdge Technologies). Temperature of the single crystal could be varied from 10 to 1000 K. A Pt sensor and a K-type thermocouple are attached to the mounting copper plate near to the Ru(0001) crystal to measure the temperature. The RAIRS experiments were performed using a VERTEX 70 FT-IR spectrometer from Bruker Optik GmbH. For this, the IR beam was taken out from the spectrometer and focused (using a combination of a paraboloidal gold-coated mirror and a plane mirror) on the single crystal at an $80 \pm 7°$ incident angle through a KBr window. The reflected IR beam from the Ru(0001) single crystal was collected by another gold-coated ellipsoidal mirror,

and finally focused onto an external liquid nitrogen cooled mercury−cadmium−telluride (MCT) detector. The IR beam path outside the vacuum system and in the IR spectrometer itself were purged with dry N_2 and high pure Ar, respectively.

Both dichloromethane (CH_2Cl_2) and d_2-dichloromethane (CD_2Cl_2) were purchased from Sigma-Aldrich (purity: 99.99%) and were further purified by several freeze−pump−thaw cycles. Deionized triply distilled water (H_2O) was used for the measurement, which was also purified through several freeze−pump−thaw cycles before introducing into the UHV chamber. Sample lines were connected to a rotary pump and were pumped before introducing the samples into the UHV chamber. At the time of the experiment, samples were introduced into the scattering chamber using leak valves and were vapor-deposited on a cold Ru(0001) single-crystal target (at 80 K). Ru(0001) single crystal was cleaned properly by repeatedly heating to 1000 K. Sample inlet tubes were kept very close to the single crystal to achieve uniform growth of the molecular solids. The deposition of molecular solids was controlled through leak valves, and monolayer coverage was evaluated assuming that 1.33×10^{-6} mbar.s = 1 ML which has been estimated to contain ∼1.1×10^{15} molecules/cm^2.[34] Temperature-dependent RAIRS was performed for the present study. Temperature was ramped @ 1 K/min and 5 min time delay was given for each temperature, before measuring each spectrum. All spectra given here were averaged for 512 scans and the spectral resolution was 4 cm^{-1}.

■ RESULTS AND DISCUSSION

1. Dichloromethane Phase Transition. The experiments were performed in several stages. To begin with, the phase transition of dichloromethane was investigated using RAIRS. Initially, 50 ML of CH_2Cl_2 was deposited on the Ru(0001) single crystal at 80 K. RAIR spectra were collected at regular intervals after warming the sample to a particular temperature (at a rate of 1 K/min), which was maintained for 5 min before collecting the spectrum. Five different vibrational modes of CH_2Cl_2 molecules positioned at ∼3050 cm^{-1} ($−CH_2$ antisymmetric stretching), ∼1265 cm^{-1} ($−CH_2$ wagging), ∼895 cm^{-1} ($−CH_2$ rocking), 748 cm^{-1} ($−CCl_2$ antisymmetric stretching), and 705 cm^{-1} ($−CCl_2$ symmetric stretching) have been detected in the RAIR spectrum at 80 K (see Supporting Information Figure S1). Among those vibrational modes, only $−CH_2$ wagging mode and $−CCl_2$ antisymmetric stretching modes are intense, which have been analyzed in detail in the subsequent investigations. Figure 1 illustrates the results obtained from 50 ML of CH_2Cl_2. At 80 K, CH_2Cl_2 showed two sets of intense broad infrared bands, due to the $−CH_2$ wagging mode and the $−CCl_2$ antisymmetric stretching mode. As the temperature was increased to 95 K, a spectral change was observed: (i) the $−CCl_2$ antisymmetric stretching peak, which was broad at 80 K, became narrow and was shifted to ∼740 cm^{-1} with a drastic increase in intensity (see Figure 2a), and (ii) the broad $−CH_2$ wagging mode was split into two peaks arising at a higher (∼1277 cm^{-1}, named as peak 1) and a lower (∼1257 cm^{-1}, named as peak 2) wavenumber region with a slightly increased intensity. This splitting is clearly visible from the inset of Figure 1, which shows an expanded view of the $−CH_2$ wagging region.

Such splitting of infrared spectra has been observed before in infrared spectroscopy-based phase transition studies of different molecules. For example, it is reported that a spectral change occurs for the broad O−H stretching peak of amorphous ice
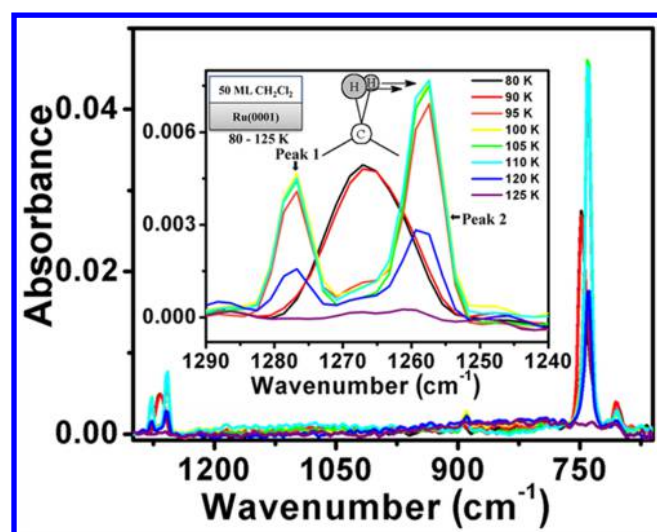
Figure 1. Temperature-dependent RAIR spectra of 50 ML CH_2Cl_2 deposited at 80 K on Ru(0001). Inset shows the expanded view of the $-CH_2$ wagging region and schematic of the surface under investigation.
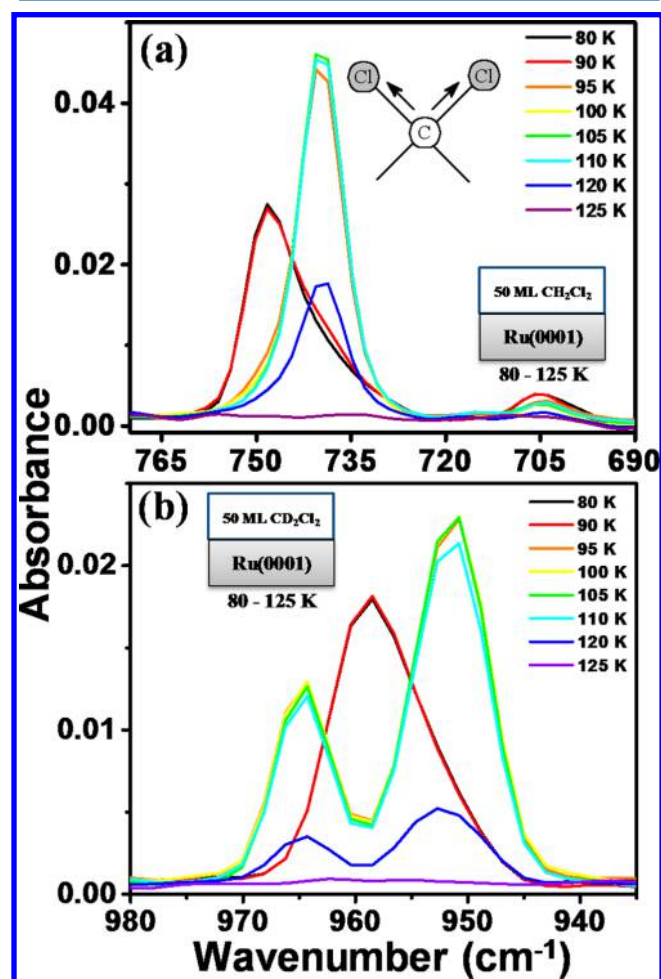

Figure 2. Temperature-dependent RAIRS study on a molecule to find changes in vibrational spectra upon heating. Spectra corresponding to (a) C−Cl antisymmetric stretching (CH_2Cl_2) mode and (b) $-CD_2$ wagging modes (CD_2Cl_2) are compared when 50 ML of CX_2Cl_2 (X = H or D) is deposited on Ru(0001) at 80 K and warmed. Insets show the schematic of the surfaces during experiment.

during crystallization of water-ice[1,35] and that a splitting of peaks was observed corresponding to both O−H and C−O stretching modes during the crystallization of methanol-ice.[36] Crystallization of methanol has been studied on highly ordered pyrolytic graphite (HOPG). Amorphous methanol deposited on HOPG surface at 97 K showed a broad O−H stretch at 3260 cm^{-1}, which split into two bands at 3290 and 3174 cm^{-1} on warming to 129 K where it underwent crystallization. Heating also leads to the splitting of the C−O stretching mode (at 1045 cm^{-1} at 97 K) giving rise to two bands at 1037 and 1027 cm^{-1}. Additionally splitting was observed in the asymmetric CH_3 stretching band. A similar study on the phase transition of vinylacetylene showed that the broad absorption band at 655 cm^{-1} (=CH_2 twisting mode) undergoes splitting during crystallization.[14] Infrared spectroscopy in transmission mode has shown that the $-CH_2$ wagging mode in the vibrational spectra of CH_2Cl_2 splits into two components in the crystalline phase.[15,37,38] Various other studies have also demonstrated such a vibrational spectral change during phase transition.[13,39] Absorption features of amorphous ices are uncharacteristically broad due to their disordered structure. When these undergo a structural change to form more stable ordered structures (crystalline) on warming, well-defined bands are seen in the infrared absorption spectra.

In the work presented herein, CH_2Cl_2 deposited on Ru(0001) at 80 K initially in amorphous form, evident from its broad absorption feature of the $-CH_2$ wagging mode (see Figure 1), is transformed into the most stable crystalline form upon warming. When the dichloromethane-ice at 95 K was cooled back to 80 K or still lower temperatures, it did not show any change in the RAIR spectrum, validating that the most stable crystalline form does not reconvert and the spectral change at 95 K is due to a phase transition. It is also noticeable from Figure 1 that further heating did not lead to any significant change in the spectrum except for the loss in intensity of the peaks due to desorption of CH_2Cl_2 at a higher temperature (~120 K). Complete desorption occurs at 125 K.

In the C−Cl stretching mode, narrowing and drastic down-shifting occur due to phase transition (Figure 2a). Splitting of the $-CD_2$ wagging region is shown in the isotopologue, CD_2Cl_2. Figure 2b shows the temperature-dependent spectra obtained for 50 ML of CD_2Cl_2 deposited on Ru(0001), applying the same strategy as described before for CH_2Cl_2. As in case of CH_2Cl_2, here also at 80 K, a broad absorption peak due to the $-CD_2$ wagging mode arises although at a much different position of ~960 cm^{-1}, and another absorption peak (not shown in the figure) is observed corresponding to the $-CCl_2$ antisymmetric mode at the same frequency as in the case of CH_2Cl_2. The former undergoes spectral change at 95 K, appearing as two peaks, one at ~964 cm^{-1} and another at ~952 cm^{-1}.

The splitting of $-CH_2/-CD_2$ wagging mode at 95 K in both CH_2Cl_2/CD_2Cl_2 is due to the factor group splitting. Factor group splitting, or Davydov splitting, is the splitting of spectral lines in a molecular crystal. Both CH_2Cl_2/CD_2Cl_2 possess C_{2v} molecular point group having four irreducible representations, namely, A_1, A_2, B_1, and B_2. They do not possess any degenerate vibrations, and therefore, in crystalline state splitting of normal modes will be due to factor group splitting which arises from interactions of vibrational modes of different molecules in a unit cell. The $-CH_2/-CD_2$ wagging mode of CH_2Cl_2/CD_2Cl_2 belonging to B_2 symmetry (in the C_{2v} point group) undergoes
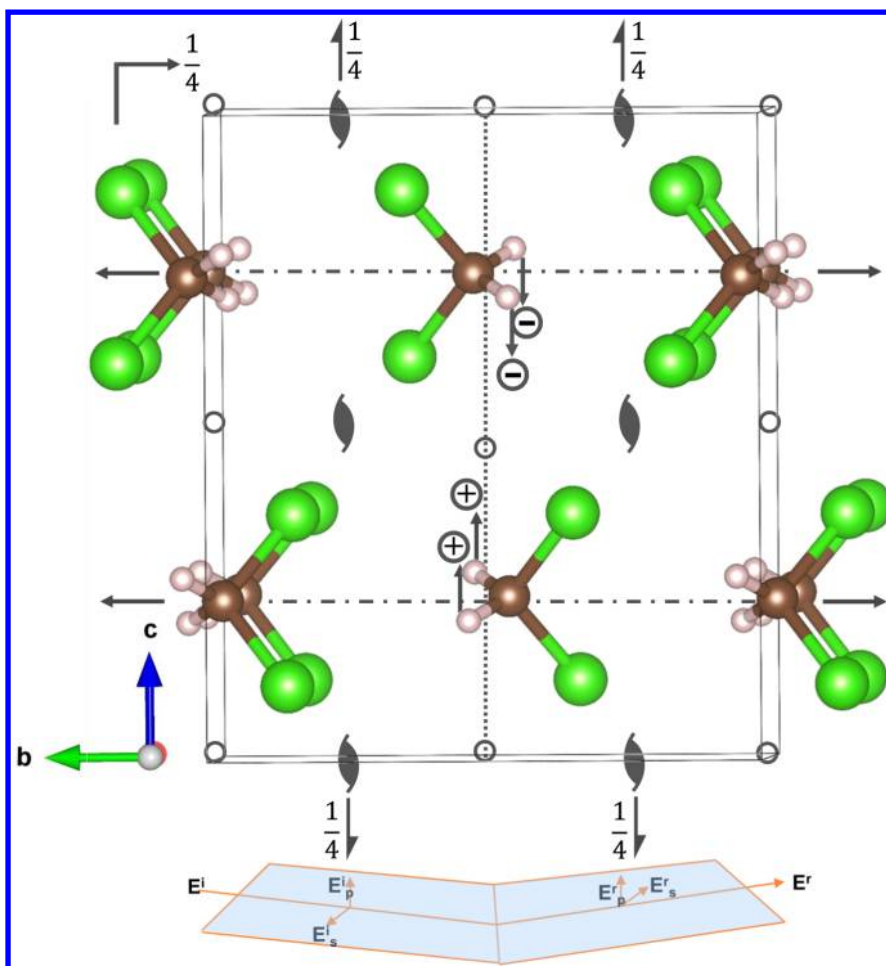
Figure 3. Crystal structure of dichloromethane: a = 4.25 Å, b = 8.13 Å, and c = 9.49 Å. Coordinates to draw the crystal structure were taken from ref 41. The crystal structure is having *Pbcn* space group. Different symmetry operations are shown in the figure. Standard notations are used to represent the symmetry operations (ref 42). The −CH$_2$ wagging mode of CH$_2$Cl$_2$ is shown with arrows and positive and negative signs. The IR beam is shown as the inset. The s- and p-components of incident (E^i) and reflected (E^r) IR radiation are also shown.

splitting in the crystalline phase. Splitting of the B$_2$ mode shows that site group in the crystalline state could be a subgroup of the molecular point group C_{2v}. Marzocchi and Manzelli[15] have found this splitting in the −CH$_2$/−CD$_2$ wagging mode of crystalline CH$_2$Cl$_2$/CD$_2$Cl$_2$ in a transmission IR measurement. From both Raman[40] and IR[15,38] study, it was concluded that dichloromethane forms orthorhombic crystals with four dichloromethane molecules per unit cell possessing *Pbcn* space group. This is shown in Figure 3. Projection of the crystal along the *a*-axis with slight tilting to show the 3D view is shown in the figure. Different symmetry operations present in the lattice are shown in the Figure 3. It shows axial glide, rotational axis, screw axis, and center of inversion operations of the lattice. The crystal structure is from Kawaguchi et al.[41] The space group of CH$_2$Cl$_2$ crystal is *Pbcn* where P stands for primitive lattice. *Pbcn* has eight equivalent positions. Due to crystal formation, symmetry of dichloromethane molecules is lowered in the crystal and they sit in the C_2 site of the crystal, and the crystallographic twofold axis passes through the C atom of the molecules. The horizontal arrows represent the twofold axis passing through the molecules. Therefore, the asymmetry unit of the structure is half of the molecules and the total unit cell content is 8 × 1/2 = 4 molecules. In the C_2 site group, A$_1$ and A$_2$ modes of C_{2v} go into A. The B$_1$ and B$_2$ modes go into B. The splitting of the vibrational band could be explained in the

following way. One CH$_2$Cl$_2$ sitting at a C_2 site (B symmetry) interacts with another CH$_2$Cl$_2$ (C_2 site, B symmetry) in the D_{2h} lattice to cause the vibrational band splitting. The split bands can be a combination of C_2, B symmetry vibrations.

Splitting of −CH$_2$ antisymmetric (∼3050 cm^{-1}) peak was also observed (see Supporting Information Figure S1), but peak intensity was very low. So we did not carry out any further analysis on this peak. There could also be splitting in the −CH$_2$ rocking mode, but it was not visible in the spectra, maybe due to lack of significant intensity. But shift in this peak to lower wavenumber side was observed. However, splitting was not observed in −CCl$_2$ antisymmetric stretching mode which is consistent with the result obtained by Marzocchi and Manzelli.[15] They showed in a polarization-dependent study that the −CH$_2$ wagging mode split in two differently polarized light, whereas splitting in −CCl$_2$ antisymmetric stretching mode occurs only in one polarized light. A similar result was observed by Brown et al. in which they have measured infrared spectra of CH$_2$Cl$_2$ single crystal in two different polarizations.[37] However, it may be noted from these studies that both the modes are infrared-active in two different polarized light. Our observation is very similar to these studies. We observed splitting only in the −CH$_2$/−CD$_2$ wagging mode, and no splitting was observed in −CCl$_2$ antisymmetric mode. Although unpolarized light was used in our measurements, RAIRS allows

only the p-component of the incident infrared beam to interact with the molecules. Although both −CH$_2$ wagging and −CCl$_2$ antisymmetric modes are active toward the p-component of the incident beam, the preferential interaction of p-component leads to the splitting of −CH$_2$ wagging mode upon phase change, whereas −CCl$_2$ antisymmetric mode does not show such a split. We have only noticed an increase in intensity of −CCl$_2$ antisymmetric mode with a red shift in the peak position upon phase transition. The exact reason for the absence of splitting in the −CCl$_2$ antisymmetric mode remains unclear. However, we assume that the orientation of crystallites with respect to incident IR light is such that it does not allow the p-component of the beam to split the −CCl$_2$ antisymmetric mode. It has been shown that orientation of crystal with respect to polarized light is important in factor group slitting.[43] The s-component incident beam could cause splitting of −CCl$_2$ antisymmetric mode, but this is not possible to be seen in RAIRS.

Large increase in intensity of −CCl$_2$ antisymmetric stretching mode was observed during phase transition. This increase in intensity in the crystalline state is due to the following reason. In the amorphous state of CH$_2$Cl$_2$, due to its randomly oriented structure, only a few C−Cl bonds are interacting with the p-component of the incident IR beam. But in the crystalline state, molecules get aligned in such a way that more C−Cl bonds could interact with the p-component of the incident IR beam, which contribute to the increase in intensity. There is an increase in intensity of the −CH$_2$ wagging mode also during phase transition along with the splitting which may be due to a similar reason.

In Figure 4, thickness- or coverage-dependent spectra of CH$_2$Cl$_2$ and CD$_2$Cl$_2$ in the −CH$_2$/−CD$_2$ wagging region at 95 K are shown. The same experimental conditions were maintained for each coverage; CH$_2$Cl$_2$ and CD$_2$Cl$_2$ films were generated on Ru(0001) surface at 80 K and heated to the desired temperature, ranging from 80 to 125 K. At all the coverages, the splitting occurred at 95 K, and therefore, only these spectra are presented in Figure 4. The figure clearly shows that, with increasing monolayer coverage, the intensities of both the peaks increase for both CH$_2$Cl$_2$ and CD$_2$Cl$_2$, though peak 2 is always more intense than peak 1. It is anticipated that, as CH$_2$Cl$_2$ or CD$_2$Cl$_2$ thickness increases, larger crystallites are formed. In large crystals, CH$_2$Cl$_2$ molecules are aligned in such a way that more −CH$_2$ bonds can preferably interact with the p-component of the IR beam and cause an increase in intensity. Moreover, with increase in monolayer coverage, the number of molecules is increased, which will also lead to an increase in peak intensity. For 10 ML coverage in both CH$_2$Cl$_2$ and CD$_2$Cl$_2$ splitting in the −CH$_2$ wagging mode was not observed. However, splitting of the peak was observed from 25 ML onward in both the cases (see Figure 4). This indicates that small coverage is not sufficient enough to form a regular crystal, whereas at relatively higher coverages regular crystals are formed which cause the splitting in the −CH$_2$ wagging mode. From the figure(s) it is also noticeable that relative increase in intensity of peak 2 is more compared to the peak 1, which indicates that peak 2 is more sensitive to monolayer coverage. We find that degree of splitting is more in the case of CH$_2$Cl$_2$ compared to CD$_2$Cl$_2$. After splitting, the −CH$_2$ wagging mode of CH$_2$Cl$_2$ peaks appear in the range of ∼1250−1285 cm^{-1}, corresponding to a total base width of ∼35 cm^{-1}, while for CD$_2$Cl$_2$ the CD$_2$ wagging mode peaks span the range from ∼942 to ∼972 cm^{-1}, a total base width of 30 cm^{-1}. This
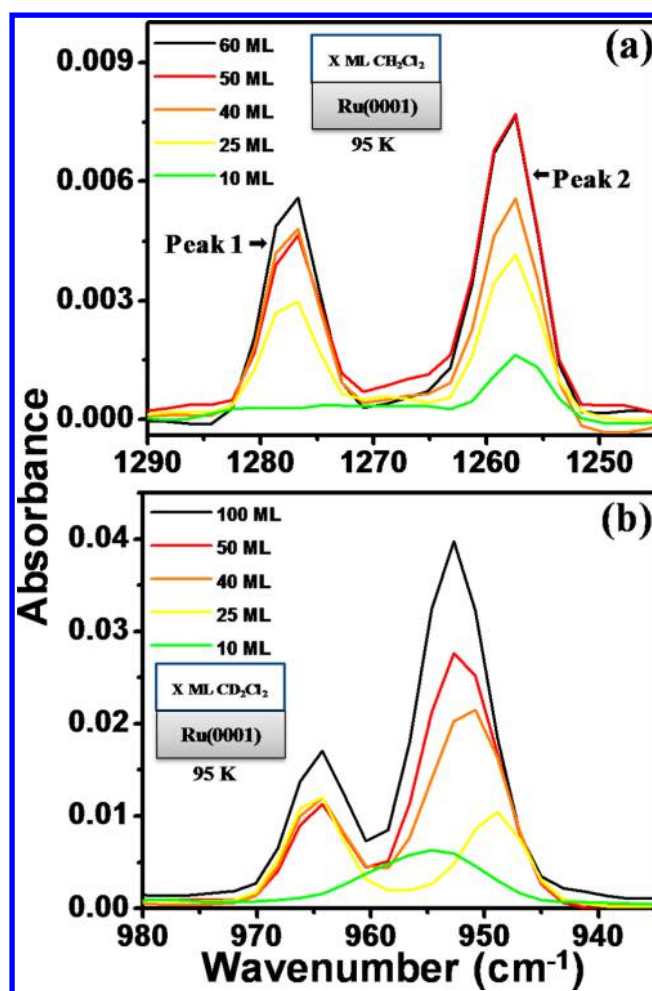
Figure 4. RAIR spectra in the (a) −CH$_2$ wagging region of CH$_2$Cl$_2$ and (b) −CD$_2$ wagging region of CD$_2$Cl$_2$ for various coverages at 95 K. Inset gives the schematic of the surfaces.

difference in splitting is a result of the isotope effect. Thus, shift due to intermolecular interaction in CH$_2$Cl$_2$ crystal is likely to be more than in CD$_2$Cl$_2$.

2. Crystallization of Dichloromethane within ASW Pores. In the next set of experiments, ASW was condensed on the CH$_2$Cl$_2$ film to investigate its role on the crystallization process of the underlying CH$_2$Cl$_2$ layers. At first, 20 ML of ASW was deposited on top of 50 ML of CH$_2$Cl$_2$ on Ru(0001) at 80 K and temperature-dependent RAIRS was performed on this system. The results obtained are shown in Figure 5a. A schematic of the surface is shown in the inset of the figure. This is given just to show the deposition of a distinct layer. The structure may be different at the interface with significant intermixing. It is hard to study interfacial morphology in the current investigation. However, during overlayer deposition, we have given sufficient time between subsequent depositions so that the layers are likely to form one after another. From the figure, it is clear that spectra at 80 and 90 K look similar to those of pure CH$_2$Cl$_2$ at the same temperatures (Figure 1). But a dramatic change in the spectrum is observed at 95 K; peak 2 of −CH$_2$ wagging mode, which is the most intense peak for pure CH$_2$Cl$_2$, appears with lesser intensity than peak 1 in the presence of water-ice. There is no change in the temperature of phase transition, which occurs at 95 K. In a previous study, it was reported that CH$_2$Cl$_2$ can diffuse through ASW.[19]
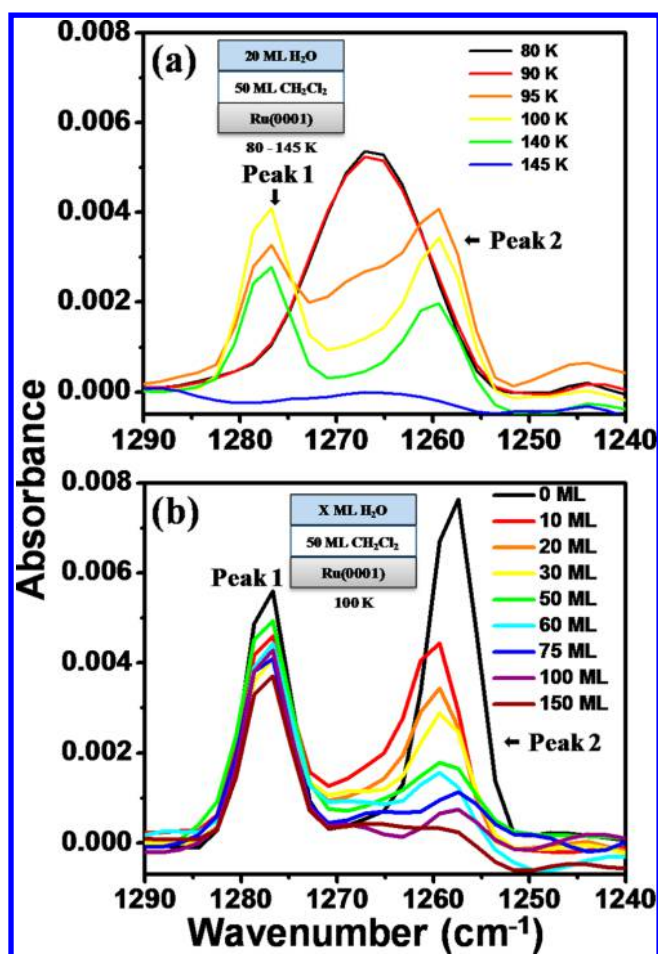
**Figure 5.** Change in $-CH_2$ wagging mode of 50 ML CH_2Cl_2 film was compared when (a) 20 ML of H_2O molecule is condensed over it at 80 K and annealed to 145 K; (b) overlayer converges of H_2O film was varied from 10 − 150 ML at 100 K. Insets show the schematic of the surfaces and the film thickness. Both CH_2Cl_2 and H_2O were deposited at 80 K on Ru(0001) surface and heated to desired temperature.

Therefore, this change in intensity of $-CH_2$ wagging mode during crystallization of CH_2Cl_2 under ASW may be due to the diffusion of CH_2Cl_2 through ASW and its crystallization inside the water-ice pores. It is also noticeable from Figure 5a that complete splitting of $-CH_2$ wagging mode due to crystallization of CH_2Cl_2 occurs at a relatively higher temperature (∼100 K) than for pure CH_2Cl_2. Furthermore, desorption of dichloromethane under amorphous water-ice takes place at 145 K (vs 125 K for pure CH_2Cl_2) when amorphous water-ice is converted into crystalline phase. This indicates that dichloromethane molecules are trapped inside the water-ice pores via diffusion which undergoes crystallization therein. As ASW crystallizes at 145 K, the water molecules reorient themselves such that it opens up a path for the trapped dichloromethane molecules to desorb. Trapping of molecules inside water-ice and their desorption during crystallization of water-ice has been reported previously and is termed as "molecular volcano".[18] However, this caging or trapping of molecules inside water pores has initially been observed by Livneh et al. and mentioned as "explosive" desorption.[44]

Additional experiments were carried out to understand this process in detail. About 50 ML of dichloromethane was deposited on Ru(0001), and the thickness of the water overlayer on top of it was varied from 10 to 150 ML. It was found that crystallization of CH_2Cl_2 took place at the same temperature (∼100 K) regardless of the water overlayer coverage. The variation of RAIR spectrum in the $-CH_2$ wagging mode region for 50 ML of CH_2Cl_2 at 100 K as a function of different overlayer coverages of water is illustrated in Figure 5b. The figure shows that at 10 ML of water-ice coverage, the intensity of peak 2 at ∼1257 cm^{-1} was drastically reduced compared to that of pure CH_2Cl_2. Further addition of the water-ice overlayer decreased its intensity continuously, such that it almost vanished at 150 ML of ASW coverage. Corresponding correlation is evident from Figure 6 where the
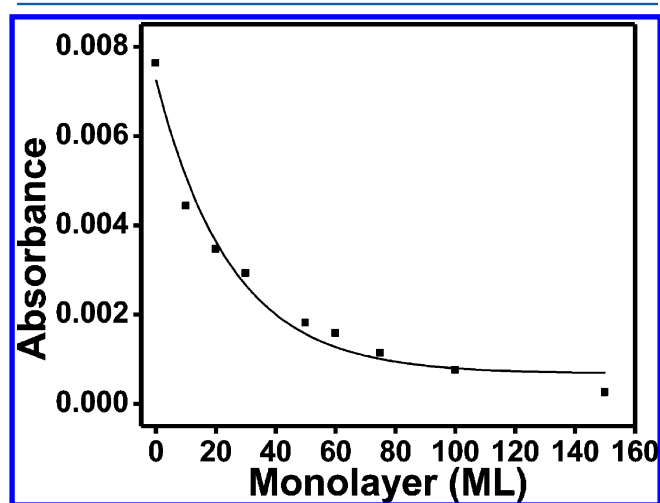
**Figure 6.** Intensity of peak 2 at 100 K is plotted against monolayer coverage of water.

maximum intensity of peak 2 at 100 K, taken from Figure 5b, is plotted against the monolayer coverage of water-ice. From the plot we see that the peak intensity follows an exponential decrease. Initially, at lower coverage, say for 50 ML of water, the intensity drop was significant, which slows down with coverage. This could be because of two reasons. First, as water-ice coverage is increased, it forms thicker layers and CH_2Cl_2 molecules have to travel longer distances. Second, with increase in water-ice coverage, availability of CH_2Cl_2 molecules for diffusion decreases as most of the molecules have occupied accessible pores. In this diffusion process, CH_2Cl_2 exists in two different states. A fraction of CH_2Cl_2 molecules diffuses within the pores of water-ice, and another fraction of molecules still remains under the water-ice. The number of molecules present under water-ice decreases as the coverage of the latter is increased due to increase in the diffusing fraction of CH_2Cl_2. From Figure 5a it is also noticeable that the peak intensity of $-CH_2$ wagging mode at 80 and 90 K is the same which is almost equal in intensity of pure CH_2Cl_2 (Figure 1, inset). A decrease in intensity of the peak is observed only during crystallization of CH_2Cl_2. This indicates that diffusion of CH_2Cl_2 molecules through water-ice is much faster at the crystallization temperature. Just before the crystallization temperature, molecular motion of CH_2Cl_2 increases due to their reorganization which causes the diffusion to be faster. It is not that crystalline CH_2Cl_2 is diffusing; rather, the individual molecular entities are diffusing before crystallization. This reorganization may force CH_2Cl_2 molecules to diffuse into the water-ice pores and crystallize in the confined environment and essentially form small crystals or irregular crystals inside the pores It is also noticeable that crystallization of CH_2Cl_2 is

delayed when covered with ASW (~100 K) compared to pure CH_2Cl_2. The microporous structure of water-ice in this temperature range may also facilitate diffusion. Such a structure may create a number of connected pathways through which CH_2Cl_2 molecules can diffuse. Interaction of both the molecules can also play a significant role in the diffusion process. Yan and Chu suggested that H-bond interaction between water molecules is weaker than that between oxalic acid and water.[45] In the CH_2Cl_2–ASW system, there could also be H-bonding between CH_2Cl_2 and water-ice, and the H-bonding interaction is likely to be stronger than that between CH_2Cl_2. This interaction may also lead to an enhancement in the diffusion process. The formation of small or irregular crystals inside the pores of water-ice is further supported by Figure S2, in which the antisymmetric –CCl_2 stretching region of 50 ML of CH_2Cl_2 is shown at different coverages of water-ice at 100 K. A continuous decrease in intensity of this peak for a constant coverage of CH_2Cl_2 was observed upon increase in coverage of water-ice. However, the peak appears at the same position as it appears in pure crystalline CH_2Cl_2. This suggests that CH_2Cl_2 diffuses and crystallizes subsequently inside the water-ice pores and the crystals are randomly oriented within the pores. Due to the random orientation of the crystallites, the availability of C–Cl bonds to interact with the p-component of the beam gets reduced. As the water-ice coverage is increased, diffusion of CH_2Cl_2 is also increased, and more randomly oriented crystallites are formed. Randomness in the crystallite orientation causes greater reduction in intensity.

As mentioned previously, with increase in water-ice coverage, larger fraction of molecules diffuse within the water-ice pores through the microporous channels and the fraction under water-ice is decreased. Inside the water-ice pores, in the confined environment, it crystallizes as a small crystal or irregular crystal. Hence, with increase in water-ice coverages, more and more water-ice pores are occupied with CH_2Cl_2. Due to the formation of irregular crystallites within the pores of water-ice, interactions between the same molecular entities are not regular and they are not strong enough to contribute to the increase in intensity. Also different orientations of irregular crystals within the pores of water-ice can reduce or cancel interactions. We have mentioned that splitting in –CH_2 wagging mode is due to the interaction of vibrational modes of different molecules in the crystal. If dimensions of the crystallites are small or they are irregular within the pores of water-ice, interaction between the vibrational modes will be reduced. In the previous study done of Lagaron, it was concluded that relative intensity of the factor group split peak reduces due to lack of crystallinity.[46] Formation of disordered and ill-defined crystallites reduce the relative intensity of the split peak.[46] This supports our argument. At 150 ML almost all the CH_2Cl_2 molecules are diffused through the pores of water-ice, which means the fraction of molecules below water-ice has almost vanished. The diffused molecules crystallize inside the pores of water-ice and the crystallite size of CH_2Cl_2 is sufficiently small to have essentially no interaction between the equivalent molecular entities within the crystal, and peak 2 disappears completely. One point should be noted here is that RAIRS measurements cannot distinguish the two different states of CH_2Cl_2 molecules (diffused within water-ice and buried under it) as it probes all the molecules present in the system. But we could see a continuous decrease of peak 2 intensity with the formation of more and more irregular crystals within water-ice pores. Due to the absence of large crystals

inside ASW pores, we see no contribution to the intensity of peak 2. Major contribution to the intensity of peak 2 comes from molecules staying at the bottom of ASW (Ru@CH_2Cl_2@H_2O system). The CH_2Cl_2 molecules at the bottom form large crystals and cause the splitting of the peaks and contribute to the intensity of peak 2. However, as water-ice coverages are increased, more CH_2Cl_2 molecules are diffused and the crystal dimension at the bottom is also reduced causing the gradual reduction in intensity of peak 2. Therefore, it may be concluded that intensity of peak 2 depends on the crystal dimensions, which in turn is related to the pore volume of ASW. However, intensity of peak 1 remains. This intensity comes from the –CH_2 wagging mode of the crystalline or irregularly crystalline CH_2Cl_2. Here, molecules present in the system as a whole contribute to the intensity of peak 1. Therefore, even though splitting is absent due to diffusion and formation of irregular crystals, we observe peak 1. Its intensity is reduced to some extent due to random orientation of the irregular crystals inside the pores, although it appears as the most intense peak at all the coverages among the split –CH_2 modes. In a pure crystalline state, strong interaction induces splitting of the –CH_2 wagging mode along with an increase in intensity.

3. Control Experiments to Validate the Diffusion Hypothesis. *3.a. IR Spectroscopic Studies.*

To validate this hypothesis of diffusion followed by crystallization inside water pores which decreases the intensity of peak 2, we have performed a few sets of control experiments. In the first set, ASW was deposited on crystalline CH_2Cl_2. For this, 50 ML of CH_2Cl_2 was deposited on Ru(0001) at 80 K, heated to 95 K to make it crystalline, and cooled back to 80 K with a subsequent deposition of H_2O on top of crystalline CH_2Cl_2. The temperature of this system was then increased in steps from 80 to 150 K. Figure 7a displays the temperature-dependent RAIR spectra obtained from this study. Initially, the 50 ML of CH_2Cl_2 on Ru(0001) at 80 K was in an amorphous state, and upon heating it underwent a phase transition at 95 K (see the inset in Figure 7a) as can be seen from the splitting of the –CH_2 wagging mode, similar to that seen in Figure 1. Subsequent deposition of H_2O at 80 K forming the ASW layer did not cause the intensity of peak 2 (1257 cm^{-1}) to become less than that of peak 1, as opposed to the case of the amorphous CH_2Cl_2–ASW system (Figure 5). Peak intensity at 80 K after crystallization and 95 K after water-ice overlayer deposition remained unchanged, implying that crystalline CH_2Cl_2 due to its ordered structure does not diffuse through ASW. Phase transition releases energy into the system which may induce desorption of molecules from the surface. Therefore, during crystallization, CH_2Cl_2 releases some energy, which causes desorption of some CH_2Cl_2 molecules on the surface. This could be the reason for the small reduction in peak intensity for crystalline CH_2Cl_2 at 80 K when water was deposited. This reduction in intensity is shown by both peak 1 and peak 2. However, the peak intensities at 80 and 95 K after ASW deposition are same. This validates our proposition that the decrease in the intensity of –CH_2 wagging mode at 1257 cm^{-1}, for amorphous CH_2Cl_2 deposited under ASW, is due to the diffusion of CH_2Cl_2 inside water-ice pores. However, such a diffusion is not uniform and it leads to the formation of small crystals or irregular crystals inside ASW, which results in decrease of molecular interaction in the unit cell. The crystalline CH_2Cl_2 formed in ASW can desorb only at 145 K when water undergoes crystallization. Hence, there is no
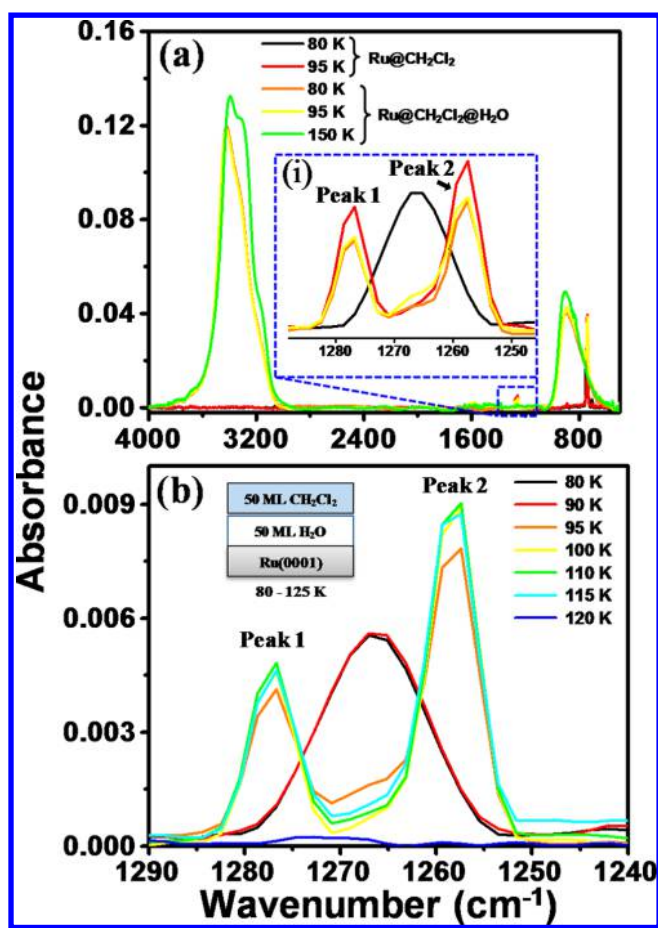
Figure 7. (a) Temperature-dependent RAIR spectra for 50 ML of amorphous H_2O deposited on 50 ML of crystalline CH_2Cl_2. CH_2Cl_2 was initially deposited at 80 K (black), subsequently heated to 95 K to result in crystallization (red), and cooled back to 80 K (light green), and then 50 ML water was deposited on top and temperature-dependent RAIR spectra were collected. Inset (i) shows an enlarged view of $-CH_2$ wagging mode. (b) Temperature-dependent RAIR spectra for 50 ML of CH_2Cl_2 which was deposited on top of 50 ML of ASW at 80 K.

change in $-CH_2$ wagging mode intensity here until desorption occurs.

In the second set of control experiments, temperature-dependent RAIR spectra were collected for 50 ML of CH_2Cl_2 deposited on top of 50 ML of ASW at 80 K. From Figure 7b, it is clear that, when CH_2Cl_2 is deposited on top of water-ice, it behaves like a pure CH_2Cl_2 film, undergoing crystallization at 95 K and desorbing from the water surface at 125 K, having no decrease in the intensity of peak 2. This confirms that when CH_2Cl_2 is on top of water there is no diffusion or mixing with water-ice. The nonoccurrence of CH_2Cl_2 diffusion through underlying ASW may be due to the surface property of both the species. CH_2Cl_2 does not wet the ASW surface properly, and hence, molecules do not get into the pores of ASW resulting in hindrance to diffusion. As suggested previously, CH_2Cl_2 diffusion in the overlaid ASW deposition could be due to molecular motion during phase transition. The control experiment where ASW was overlaid on crystalline CH_2Cl_2 where no diffusion was observed supports this argument. Disordered structure of amorphous CH_2Cl_2 can diffuse through the microporous channel of ASW, whereas ordered crystalline state of CH_2Cl_2 cannot diffuse. It is also likely that the pores in

the topmost layer of ASW got closed as CH_2Cl_2 was deposited which prevents the latter's diffusion.

Although adsorption could occur on condensed water, this cannot be attributed to be the reason for observed changes in peak. CH_2Cl_2 deposited over ASW ($Ru@ASW@CH_2Cl_2$) behaved similarly to pure CH_2Cl_2 ($Ru@CH_2Cl_2$) upon phase change and underwent desorption at 120 K. Thus, the observed changes in the IR spectra are due to deposition of ASW over CH_2Cl_2 ($Ru@CH_2Cl_2@ASW$) allowing the latter to diffuse into the pores of ASW. Adsorption of CH_2Cl_2 on condensed water cannot be concluded as the reason for the change as it does not happen in $Ru@ASW@CH_2Cl_2$. Spectrum of 1 ML of CH_2Cl_2 could not be measured as the intensity was weak. This was further confirmed by TPD measurements, to be described later.

3.b. Low-Energy Cs^+ Scattering. The diffusion of CH_2Cl_2 through water-ice was additionally investigated by Cs^+ scattering. Low-energy (<100 eV) Cs^+ scattering is a very powerful surface-sensitive technique. The top layers of molecular surfaces can be probed by this technique. Here, low-energy Cs^+ are allowed to collide on the surface and the scattered ions are analyzed using a mass spectrometer. Species present on the surface can easily be identified by this technique. Therefore, to get the surface information, we have performed Cs^+ scattering of various samples. This will provide a clearer picture of the diffusion process. Figure 8 represents the Cs^+ scattering spectra from four different experiments at 95 K. In all these cases, deposition was done at 80 K and samples were annealed to 95 K before Cs^+ scattering. Schematics of the surfaces are shown in the inset of the figure. Collision energy of the Cs^+ was 40 eV. Figure 8a represents the scattering spectrum of pure CH_2Cl_2 where the presence of CH_2Cl_2 on the surface can be confirmed from the peaks at m/z 49 and 84, assigned to CH_2Cl^+ and $CH_2Cl_2{}^+$, respectively, and also the Cs adduct products of the corresponding species at m/z 182 and 217 $[Cs(CH_2Cl)^+$ and $Cs(CH_2Cl_2)^+$, respectively]. An enlarged spectrum is shown in the inset of Figure 8a to show the isotopic pattern of the ions which again confirms the identity of the species. In the next set of experiments, 50 ML of CH_2Cl_2 was covered with 50 ML of D_2O followed by Cs^+ scattering. Figure 8b shows the spectrum due to this experiment where the surface species corresponding to both D_2O and CH_2Cl_2 were detected. The spectrum shows the peaks at m/z 22, 42, 49, and 84 due to D_3O^+, $D_5O_2{}^+$, CH_2Cl^+, and $CH_2Cl_2{}^+$, respectively, and Cs adduct products at m/z 153, 173, 182, 193, and 217 due to $Cs(D_2O)^+$, $Cs(D_2O)_2{}^+$, $Cs(CH_2Cl)^+$, $Cs(D_2O)_3{}^+$, and $Cs(CH_2Cl_2)^+$, respectively (with isotopically resolved peaks in the inset). Thus, even though a CH_2Cl_2 layer was covered with D_2O-ice, the Cs^+ scattering was able to detect CH_2Cl_2. This indicates the diffusion of CH_2Cl_2 molecules and their presence on the surface. It might be noted that Cs^+ scattering at this collision energy can probe 1−5 ML of the top surface. The CH_2Cl_2 molecules below diffuse through the porous structure of D_2O and reach the surface which are picked up by the Cs^+. The same experiment was repeated by increasing the coverage of D_2O from 50 to 100 ML, keeping the CH_2Cl_2 coverage constant at 50 ML. Here also we see the appearance of CH_2Cl_2 molecules on the surface, but the intensities of the peaks reduce considerably compared to the 50 ML D_2O overlayer deposition. This suggests that the presence of surface species has reduced due to the increased overlayer thickness of D_2O. All the features of CH_2Cl_2 on the surface disappear with further increase in the overlayer thickness of D_2O to 500 ML (Figure
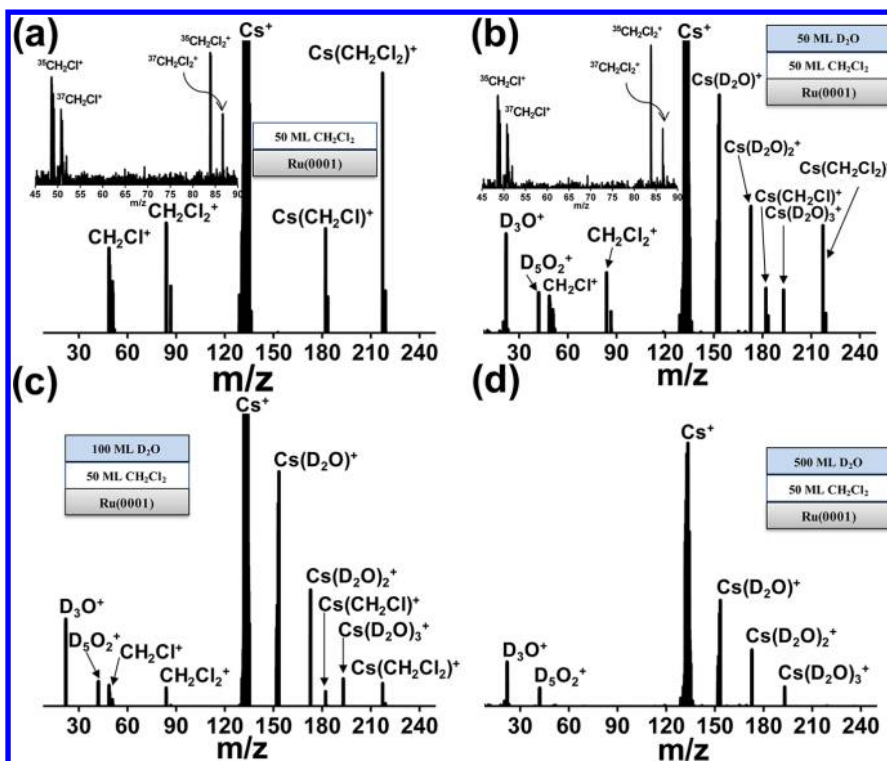
Figure 8. 40 eV Cs$^+$ collision on (a) Ru@50 ML of CH$_2$Cl$_2$, (b) Ru@50 ML of CH$_2$Cl$_2$@50 ML of D$_2$O, (c) Ru@50 ML of CH$_2$Cl$_2$@100 ML of D$_2$O, and (d) Ru@50 ML of CH$_2$Cl$_2$@500 ML of D$_2$O. Depositions were done at 80 K, and Cs$^+$ scattering was performed at 95 K.

8d). These results support our suggestion that, due to diffusion, the CH$_2$Cl$_2$ molecules get into the pores of water-ice and a fraction of molecules also reaches the surface at lower water-ice coverage. As the water-ice coverages are increased, the CH$_2$Cl$_2$ molecules have to a travel longer distances to reach the surface, and at certain coverage, the distance is sufficiently high for the molecules so that they cannot reach the surface. Here, all the diffused molecules get trapped within the pores of water-ice.

3.c. TPD Measurements. We have performed TPD experiments for three different sets of samples to have a definite conclusion of the diffusion process. In all the experiments, the molecules were deposited at 80 K and ramping of 10 K/min was used to measure the TPD spectra. To obtain TPD spectra, m/z 49 (CH$_2$Cl$^+$) for CH$_2$Cl$_2$ and m/z 20 (D$_2$O$^+$) for D$_2$O were selected. The TPD spectrum of 50 ML of CH$_2$Cl$_2$ shows a desorption peak maximum at ~122 K (Figure 9a), in accordance with the IR measurements in which a decrease in spectral intensity at ~120 K and complete disappearance of the peaks at 125 K were seen. CH$_2$Cl$_2$ molecules deposited on top of ASW also show similar behavior. When CH$_2$Cl$_2$ was deposited over ASW, three distinct peaks in the TPD spectrum with peak maxima at ~122, 145, and 160 K were seen (Figure 9b). In this experiment, 50 ML of CH$_2$Cl$_2$ was deposited on top of 50 ML of D$_2$O at 80 K, and during TPD, the temperature was ramped at 10 K/min. While most of the molecules desorb at ~122 K, a fraction desorbs at relatively higher temperatures.

The peak at ~145 K corresponds to the first monolayer of CH$_2$Cl$_2$ molecules which are adsorbed on ASW.[20] This monolayer has strong interaction with ASW via H-bonding or through molecular interactions. Therefore, desorption of these molecules from the ASW surface occurs at a relatively higher temperature when ASW undergoes a structural change (amorphous to crystalline transition). Due to the structural change, water molecules rearrange themselves and the
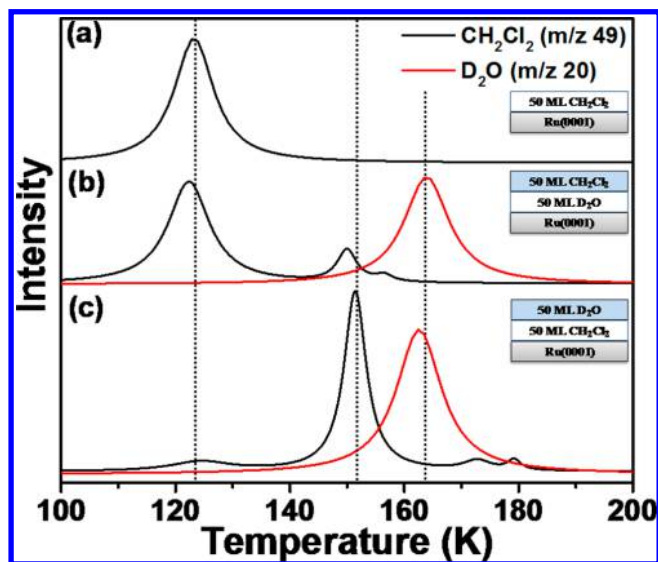
Figure 9. TPD spectra of (a) Ru@50 ML of CH$_2$Cl$_2$, (b) Ru@50 ML of D$_2$O@50 ML of CH$_2$Cl$_2$, and (c) Ru@50 ML of CH$_2$Cl$_2$ @ 50 ML of D$_2$O. Dotted lines are given to show the peak maxima. All the depositions were done at 80 K, and ramping rate was 10 K/min.

interaction between ASW and CH$_2$Cl$_2$ is reduced which causes desorption of the molecules. A smaller fraction of molecules is trapped in the pores of water-ice near the surface and desorbs at an even higher temperature (near to 160 K). These trapped molecules themselves desorb when water itself starts desorbing. From this study we can conclude that CH$_2$Cl$_2$ deposited on top of ASW does not diffuse through the pores of ASW, rather stays on the surface and gets crystallized. Crystallization is evident from the IR spectra (Figure 7). In our present IR measurement, it was not possible to get spectra from monolayer coverage of

CH_2Cl_2 due to poor intensity; therefore, even though a small fraction of molecules was present on the surface of ASW, we observed complete disappearance of IR intensity and concluded that CH_2Cl_2 deposited on top of ASW behaves like pure CH_2Cl_2. TPD experiment also supports the argument. In another set of experiments, 50 ML of CH_2Cl_2 was covered with 50 ML of D_2O and TPD spectra were measured. The results (Figure 9c) show four distinct desorption features. The broad peak with the peak maximum ~124 K is consistent with the desorption feature of pure CH_2Cl_2. This clearly manifests the diffusion of CH_2Cl_2 through ASW. Once ASW is deposited on top of CH_2Cl_2, the molecules start diffusing through the pores of ASW and get trapped there, and in this diffusion process, a small fraction of molecules reaches the surface. The surface species desorb first, and the trapped molecules desorb from the pores of ASW as molecular volcano when ASW undergoes a structural change at ~145 K. The detection of surface CH_2Cl_2 species due to diffusion was also observed in Cs^+ scattering experiment (Figure 8). Both the results agree that CH_2Cl_2 diffuses through ASW. Two low-intensity n features were observed at higher temperatures (~172 and 179 K). This indicates that still there are trapped molecules which desorb at relatively higher temperatures along with the desorption of water-ice. This trapping and desorption of molecules at higher temperature has been described previously by May et al.[47]

CONCLUSIONS

This study reveals that dichloromethane undergoes a phase transition at ~95 K prior to desorption, irrespective of its coverage. This phase transition of CH_2Cl_2 is established from the peak shift of the C−Cl antisymmetric stretching frequency at 748 cm^{-1} and a peak splitting of the −CH_2 wagging mode at 1265 cm^{-1} into two: peak 1 at 1277 cm^{-1} and peak 2 at 1257 cm^{-1}. Intensity of the both the split peaks increases with increasing CH_2Cl_2 coverage, though peak 2 is always more intense than peak 1. Once water-ice layers are deposited over a CH_2Cl_2 film, the latter diffuses through it at low temperatures and forms small crystals or irregular crystals inside the ice pores, undergoing a phase transition within. As the water-ice overlayer increases, the number of pores increases and more CH_2Cl_2 molecules diffuse through the pores resulting in the formation of more small or irregular crystals of CH_2Cl_2, and this leads to the reduction in intensity of peak 2 at 1257 cm^{-1}. Desorption of the trapped CH_2Cl_2 takes place at higher temperatures (~145 K) only after crystallization of the water-ice film. The Cs^+ scattering and TPD experiments provide additional support to the diffusion process.

ASSOCIATED CONTENT

Ⓢ Supporting Information

The Supporting Information is available free of charge on the ACS Publications website at DOI: 10.1021/acs.jpcc.6b00436.

> Temperature-dependent RAIR spectra of 50 ML CH_2Cl_2 and RAIR spectra of −CCl_2 antisymmetric stretching mode of 50 ML CH_2Cl_2 as a function of overlayer coverages of ASW at 100 K (PDF)

AUTHOR INFORMATION

Corresponding Author
*Fax: + 91-44 2257-0545. E-mail: pradeep@iitm.ac.in.

Notes
The authors declare no competing financial interest.

REFERENCES

(1) Buontempo, U. Infrared Spectra of Amorphous Ice. *Phys. Lett. A* **1972**, *42*, 17−18.

(2) Burke, D. J.; Brown, W. A. Ice in Space: Surface Science Investigations of the Thermal Desorption of Model Interstellar Ices on Dust Grain Analogue Surfaces. *Phys. Chem. Chem. Phys.* **2010**, *12*, 5947−5969.

(3) Smith, R. S.; Petrik, N. G.; Kimmel, G. A.; Kay, B. D. Thermal and Nonthermal Physiochemical Processes in Nanoscale Films of Amorphous Solid Water. *Acc. Chem. Res.* **2012**, *45*, 33−42.

(4) Shin, S.; Kang, H.; Kim, J. S.; Kang, H. Phase Transitions of Amorphous Solid Acetone in Confined Geometry Investigated by Reflection Absorption Infrared Spectroscopy. *J. Phys. Chem. B* **2014**, *118*, 13349.

(5) Burton, E. F.; Oliver, W. F. X-Ray Diffraction Patterns of Ice. *Nature (London, U. K.)* **1935**, *135*, 505−6.

(6) Zimbitas, G.; Haq, S.; Hodgson, A. The Structure and Crystallization of Thin Water Films on Pt(111). *J. Chem. Phys.* **2005**, *123*, 174701/1−174701/9.

(7) Jenniskens, P.; Blake, D. F. Structural Transitions in Amorphous Water Ice and Astrophysical Implications. *Science (Washington, DC, U. S.)* **1994**, *265*, 753−6.

(8) Jenniskens, P.; Banham, S. F.; Blake, D. F.; McCoustra, M. R. S. Liquid Water in the Domain of Cubic Crystalline Ice Ic. *J. Chem. Phys.* **1997**, *107*, 1232−1241.

(9) Bag, S.; Bhuin, R. G.; Pradeep, T. Distinguishing Amorphous and Crystalline Ice by Ultralow Energy Collisions of Reactive Ions. *J. Phys. Chem. C* **2013**, *117*, 12146−12152.

(10) Cyriac, J.; Pradeep, T.; Kang, H.; Souda, R.; Cooks, R. G. Low-Energy Ionic Collisions at Molecular Solids. *Chem. Rev. (Washington, DC, U. S.)* **2012**, *112*, 5356−5411.

(11) Bag, S.; Bhuin, R. G.; Natarajan, G.; Pradeep, T. Pradeep, T., Probing Molecular Solids with Low-Energy Ions. *Annu. Rev. Anal. Chem.* **2013**, *6*, 97−118.

(12) Zhang, Y.; Gu, M.; Zhang, T.; Yuan, Y.; Zhou, L.; Duan, Y.; Zhang, J. Phase Transition Behavior of Plla Ultrathin Film Studied by Grazing Angle Reflection Absorption Infrared Spectroscopy. *Vib. Spectrosc.* **2012**, *63*, 338−341.

(13) Zheng, W.; Kaiser, R. I. An Infrared Spectroscopy Study of the Phase Transition in Solid Ammonia. *Chem. Phys. Lett.* **2007**, *440*, 229−234.

(14) Kim, Y. S.; Kaiser, R. I. An Infrared Spectroscopic Study of Amorphous and Crystalline Ices of Vinylacetylene and Implications for Saturn's Satellite Titan. *Astrophys. J., Suppl. Ser.* **2009**, *181*, 543−547.

(15) Marzocchi, M. P.; Manzelli, P. Infrared Spectrum of Crystalline CH_2Cl_2 and CD_2Cl_2. Polarization Measurements and Crystal Structure. *J. Chem. Phys.* **1970**, *52*, 2630−9.

(16) Molina, M. J.; Tso, T.-L.; Molina, L. T.; Wang, F. C.-Y. Antarctic Stratospheric Chemistry of Chlorine Nitrate, Hydrogen Chloride, and Ice: Release of Active Chlorine. *Science* **1987**, *238*, 1253−1257.

(17) Grecea, M. L.; Backus, E. H. G.; Fraser, H. J.; Pradeep, T.; Kleyn, A. W.; Bonn, M. Mobility of Haloforms on Ice Surfaces. *Chem. Phys. Lett.* **2004**, *385*, 244−248.

(18) Smith, R. S.; Huang, C.; Wong, E. K. L.; Kay, B. D. The Molecular Volcano: Abrupt CCl_4 Desorption Driven by the Crystallization of Amorphous Solid Water. *Phys. Rev. Lett.* **1997**, *79*, 909−912.

(19) Cyriac, J.; Pradeep, T. Probing Difference in Diffusivity of Chloromethanes through Water Ice in the Temperature Range of 110−150 K. *J. Phys. Chem. C* **2007**, *111*, 8557−8565.

(20) Horowitz, Y.; Asscher, M. Electron-Induced Chemistry of Methyl Chloride Caged within Amorphous Solid Water. *J. Chem. Phys.* **2013**, *139*, 154707.

(21) Hama, T.; Watanabe, N. Surface Processes on Interstellar Amorphous Solid Water: Adsorption, Diffusion, Tunneling Reactions, and Nuclear-Spin Conversion. *Chem. Rev. (Washington, DC, U. S.)* **2013**, *113*, 8783−8839.

(22) Zubkov, T.; Smith, R. S.; Engstrom, T. R.; Kay, B. D. Adsorption, Desorption, and Diffusion of Nitrogen in a Model Nanoporous Material. I. Surface Limited Desorption Kinetics in Amorphous Solid Water. *J. Chem. Phys.* **2007**, *127*, 184707/1−184707/11.

(23) Bertin, M.; Romanzin, C.; Michaut, X.; Jeseck, P.; Fillion, J. H. Adsorption of Organic Isomers on Water Ice Surfaces: A Study of Acetic Acid and Methyl Formate. *J. Phys. Chem. C* **2011**, *115*, 12920−12928.

(24) Dohnalek, Z.; Kimmel, G. A.; Ayotte, P.; Smith, R. S.; Kay, B. D. The Deposition Angle-Dependent Density of Amorphous Solid Water Films. *J. Chem. Phys.* **2003**, *118*, 364−372.

(25) Raut, U.; Fama, M.; Teolis, B. D.; Baragiola, R. A. Characterization of Porosity in Vapor-Deposited Amorphous Solid Water from Methane Adsorption. *J. Chem. Phys.* **2007**, *127*, 204713/1−204713/6.

(26) Stevenson, K. P.; Kimmel, G. A.; Dohnalek, Z.; Smith, R. S.; Kay, B. D. Controlling the Morphology of Amorphous Solid Water. *Science (Washington, DC, U. S.)* **1999**, *283*, 1505−1507.

(27) Smith, R. S.; Zubkov, T.; Dohnalek, Z.; Kay, B. D. The Effect of the Incident Collision Energy on the Porosity of Vapor-Deposited Amorphous Solid Water Films. *J. Phys. Chem. B* **2009**, *113*, 4000−4007.

(28) Ayotte, P.; Smith, R. S.; Stevenson, K. P.; Dohnalek, Z.; Kimmel, G. A.; Kay, B. D. Effect of Porosity on the Adsorption, Desorption, Trapping, and Release of Volatile Gases by Amorphous Solid Water. *J. Geophys. Res., [Planets]* **2001**, *106*, 33387−33392.

(29) Bisschop, S. E.; Fraser, H. J.; Oberg, K. I.; van Dishoeck, E. F.; Schlemmer, S. Desorption Rates and Sticking Coefficients for Co and N₂ Interstellar Ices. *Astron. Astrophys.* **2006**, *449*, 1297−1309.

(30) Oberg, K. I.; van Broekhuizen, F.; Fraser, H. J.; Bisschop, S. E.; van Dishoeck, E. F.; Schlemmer, S. Competition between Co and N₂ Desorption from Interstellar Ices. *Astrophys. J.* **2005**, *621*, L33−L36.

(31) Cholette, F.; Zubkov, T.; Smith, R. S.; Dohnalek, Z.; Kay, B. D.; Ayotte, P. Infrared Spectroscopy and Optical Constants of Porous Amorphous Solid Water. *J. Phys. Chem. B* **2009**, *113*, 4131−4140.

(32) Mate, B.; Rodriguez-Lazcano, Y.; Herrero, V. J. Morphology and Crystallization Kinetics of Compact (HGW) and Porous (ASW) Amorphous Water Ice. *Phys. Chem. Chem. Phys.* **2012**, *14*, 10595−10602.

(33) Bag, S.; Bhuin, R. G.; Methikkalam, R. R. J.; Pradeep, T.; Kephart, L.; Walker, J.; Kuchta, K.; Martin, D.; Wei, J. Development of Ultralow Energy (1 - 10 eV) Ion Scattering Spectrometry Coupled with Reflection Absorption Infrared Spectroscopy and Temperature Programmed Desorption for the Investigation of Molecular Solids. *Rev. Sci. Instrum.* **2014**, *85*, 014103/1−014103/7.

(34) Moon, E.-S.; Kang, H.; Oba, Y.; Watanabe, N.; Kouchi, A. Direct Evidence for Ammonium Ion Formation in Ice through Ultraviolet-Induced Acid-Base Reaction of NH₃ with H₃O⁺. *Astrophys. J.* **2010**, *713*, 906−911.

(35) Smith, R. S.; Petrik, N. G.; Kimmel, G. A.; Kay, B. D. Thermal and Nonthermal Physiochemical Processes in Nanoscale Films of Amorphous Solid Water. *Acc. Chem. Res.* **2012**, *45*, 33−42.

(36) Bolina, A. S.; Wolff, A. J.; Brown, W. A. Reflection Absorption Infrared Spectroscopy and Temperature Programmed Desorption Investigations of the Interaction of Methanol with a Graphite Surface. *J. Chem. Phys.* **2005**, *122*, 044713/1−044713/12.

(37) Brown, C. W.; Obremski, R. J.; Allkins, J. R.; Lippincott, E. R. Vibrational Spectra of Single Crystals and Polycrystalline Films of CH₂Cl₂ and CH₂Br₂. *J. Chem. Phys.* **1969**, *51*, 1376−84.

(38) Kartha, V. B. Infrared Spectra of Dichloromethane, Dibromomethane, and Diiodomethane in the Solid State. *J. Mol. Spectrosc.* **1967**, *24*, 368−77.

(39) Lang, E. K.; Knox, K. J.; Momose, T.; Signorell, R. Infrared Spectroscopy and Phase Behavior of *n*-Butane Aerosols and Thin Films at Cryogenic Temperatures. *J. Phys. Chem. A* **2013**, *117*, 11745−11759.

(40) Ito, M. Raman Spectra of Polycrystalline Chloromethanes at Liquid Nitrogen Temperature. *J. Chem. Phys.* **1964**, *40*, 3128−9.

(41) Kawaguchi, T.; Tanaka, K.; Takeuchi, T.; Watanabe, T. Crystal Structure of Methylene Dichloride. *Bull. Chem. Soc. Jpn.* **1973**, *46*, 62−6.

(42) Cotton, F. A. *Chemical Applications of Group Theory*, 3rd ed.; John Wiley and Sons: New York, 1990; p 461.

(43) Marzocchi, M. P.; Bonadeo, H.; Taddei, G. Infrared Spectra in Polarized Light of Crystalline Benzene and Benzene-D₆. *J. Chem. Phys.* **1970**, *53*, 867−75.

(44) Livneh, T.; Romm, L.; Asscher, M. Cage Formation of N₂ under H₂O Overlayer on Ru(001). *Surf. Sci.* **1996**, *351*, 250−258.

(45) Yan, H.; Chu, L. T. Interactions of Oxalic Acid and Ice on Cu Surface. *Langmuir* **2008**, *24*, 9410−9420.

(46) Lagaron, J.-M. The Factor Group Splitting Phenomenon: A Vibrational Spectroscopy Approach to Assess Polymer Crystallinity and Crystalline Density. *Macromol. Symp.* **2002**, *184*, 19−36.

(47) May, R. A.; Scott Smith, R.; Kay, B. D. The Release of Trapped Gases from Amorphous Solid Water Films. Ii. "Bottom-up" Induced Desorption Pathways. *J. Chem. Phys.* **2013**, *138*, 104502/1−104502/11.